

Can Static Black Holes in Massive Gravity Serve as Candidates for Aschenbach-Like Phenomena?

Mohammad Ali S. Afshar,^{1,2,3,*} Jafar Sadeghi,^{1,2,3,†} Tahereh Azizi,^{1,‡} and A. S. Sefiedgar^{1,§}

¹*Department of Theoretical Physics, Faculty of Basic Sciences, University of Mazandaran
P. O. Box 47416-95447, Babolsar, Iran*

²*School of Physics, Damghan University, P. O. Box 3671641167, Damghan, Iran*

³*Canadian Quantum Research Center, 204-3002 32 Ave Vernon, BC V1T 2L7, Canada*

(Dated: July 22, 2025)

The Aschenbach effect is widely regarded as a manifestation of two quintessential relativistic features: frame dragging and extreme spacetime curvature. Traditionally associated with rotating geometries, this non-monotonic behavior in orbital angular velocity challenges Newtonian intuition. In our previous work, however, we demonstrated that this velocity irregularity is not exclusive to spinning spacetimes. Specifically, we showed that the presence of a stable minimum in the gravitational potential, corresponding to a stable photon sphere, can reproduce Aschenbach-like behavior in static black holes as well. This observation suggests that, even in the absence of rotational frame dragging, curvature alone—if encoded through appropriate geometric extrema—may be sufficient to induce non-monotonic velocity profiles. In this study, we build upon that foundation to investigate whether black hole architectures in theories of Massive Gravity can inherently support the emergence of Aschenbach-like phenomena. Furthermore, can this Aschenbach-like phenomenon in static configurations be considered as an observable signature in the dynamics of general relativity, similar to the original Aschenbach effect in rotating spacetimes?

Keywords: Aschenbach effect, photon spheres, Time-like Circular Orbits, black holes, Massive Gravity

I. INTRODUCTION

The Aschenbach effect, represents a compelling case of deep interplay between fundamental physics and observational astrophysics. This phenomenon is intricately tied to black hole physics, and since black holes constitute a tangible manifestation of general relativity in the physical universe, general relativity serves as the foundational framework for explaining the Aschenbach effect. The theory provides a robust mathematical structure for describing how matter and energy influence spacetime curvature within this context. In other words, The Aschenbach phenomenon is a direct prediction of general relativity in the strong-field regime, which observing it would confirm that spacetime near black holes behaves as Einstein's equations predict.

The origin of the Aschenbach effect can be traced back to pioneering investigations by researchers exploring relativistic particle motion around rotating (Kerr) black holes[1]. While the concept of frame dragging—a hallmark prediction of general relativity—had already been established [2, 3], the systematic analysis of orbital stability near Kerr black holes gained momentum in the late 20th century. Key figures such as Brandon Carter, and later Marek A. Abramowicz, made substantial contributions to the mathematical formalism underpinning these orbital dynamics[4–6]. However, in 2004, it was Aschenbach who, through numerical simulations, discovered an anomalous drop in orbital velocity for test particles extremely close to the event horizon just prior to plunge[7]. This non-monotonic behavior challenges the assumptions of traditional Keplerian flow models, often employed in simplified accretion disk theories.

The emergence of this anomalous oscillatory motion near the innermost stable circular orbit (ISCO) is notably distinct from quasi-periodic oscillations (QPOs). Unlike QPOs—which typically require magnetohydrodynamic (MHD) simulations for accretion flow modeling [8]—the Aschenbach effect is purely kinematic and appears to arise directly from Kerr geometry. Rigorous inferences from Einstein's field equations demonstrate that the phenomenon originates from the interplay between gravitational forces and rotational effects encoded in the Kerr metric. The Kerr metric, characterized by its angular momentum parameter, governs fundamental properties of rotating black holes, including ergosphere dynamics and frame-dragging. Concurrently, accretion disks around rotating black holes are regulated by complex interactions among gravitational forces, frame-dragging effects, and viscous dissipation processes [9]. Contemporary studies employing Kerr-metric-governed numerical simulations of accretion disks have successfully reproduced key aspects of the Aschenbach effect, thereby validating its theoretical underpinnings[10]. Additionally, we know that X-ray emissions from regions proximal to spinning black holes

* m.a.s.afshar@gmail.com

† pouriya@ipm.ir

‡ t.azizi@umz.ac.ir

§ a.sefiedgar@umz.ac.ir

provide crucial insights into ISCO properties[11], which are directly influenced by the spin parameter of the central object. Accordingly, based on the analysis of observations conducted using instruments such as NASA's Chandra X-ray Observatory and ESA'S XMM-Newton satellite, one can be very hopeful of obtaining spectral signatures consistent with predictions arising from the Aschenbach effect [12].

In light of the preceding discussion, it is timely to address the core question:

What, precisely, is the Aschenbach effect, and what fundamentally constitutes this effect? To answer this rigorously, we must introduce and examine the fundamental physical elements that underpin the phenomenon:

♣ The ISCO :

represents the smallest radius at which a test particle can maintain a stable circular orbit around a black hole. Beyond this threshold, orbital trajectories become unstable — minor perturbations (such as a small loss of angular momentum) trigger inward plunges.

ISCO effectively delineates the inner edge of accretion disks, Matter interior to this radius cannot sustain circular motion and undergoes rapid radial infall. In rotating (Kerr) spacetimes, ISCO properties depend on orbital orientation:

Prograde Orbits (co-rotating with spin) and Retrograde Orbits (counter-rotating)[13].

♣ Frame Dragging:

The rotation of a Kerr black hole "drags" the surrounding spacetime, altering the dynamics of nearby matter. This relativistic effect is strongest near the event horizon and weakens with distance. It is quantified by the spin parameter $a = J/M$, where J is the angular momentum and M is the mass. For maximal spin ($a/M = 1$), frame dragging reaches its extremum; for non-spinning Schwarzschild black holes ($a = 0$), the effect vanishes. Prograde orbits gain angular momentum through frame dragging, modifying expected kinematics.[13]

♣ Strong-Field Gravity:

Close to the black hole, spacetime curvature intensifies. This alters the balance between gravitational pull and centrifugal forces, leading to unexpected orbital behaviors.

♣ Orbital Angular Velocity:

Under Newtonian gravity, angular velocity Ω scales monotonically with radius as:

$$\Omega_{\text{Newton}}(r) = \sqrt{\frac{GM}{r^3}} \quad (\text{monotonically decreasing with } r).$$

This implies that as radius decreases, orbital velocity increases uniformly and vice versa.

•Kerr Angular Velocity Profile:

Near a rapidly rotating Kerr black hole, the angular velocity is given by [13]:

$$\Omega_{\text{Kerr}}(r) = \frac{\sqrt{GM} \left(r^{3/2} + a\sqrt{GM} \right)}{r^2 \left(r^{3/2} - 3\sqrt{GM}r^{1/2} + 2a\sqrt{GM} \right)}.$$

The numerator includes a spin-enhanced term $a\sqrt{GM}$ that boosts $\Omega(r)$ in prograde orbits. However, the denominator contains relativistic correction terms ($-3\sqrt{GM}r^{1/2}$) linked to intense spacetime curvature, which dampens the angular velocity at small radii.

In summary, for the Radial Evolution of $\Omega(r)$ we have:

- Phase 1 (Large r):

Keplerian-like increase in Ω as r decreases ($d\Omega/dr > 0$).

-Phase 2 (Intermediate r):

Frame-dragging dominates $\rightarrow \Omega$ rises super-Keplerianly.

- Phase 3 (Critical Radius r_{peak}):

Spacetime curvature overtakes $\rightarrow \Omega$ decreases as r decreases ($d\Omega/dr < 0$):

$$\frac{d\Omega}{dr} > 0 \quad \xrightarrow{r=r_{\text{peak}}} \quad \frac{d\Omega}{dr} < 0.$$

This unexpected reversal — the peak and drop in orbital angular velocity at close proximity to the event horizon — which is in sharp contrast with Newtonian expectations is the hallmark of the Aschenbach effect and in essence, arises from the interplay between intense gravitational curvature and spin-induced frame dragging.

Building upon our earlier discussion, we have sawed that the Aschenbach effect—manifested as a non-monotonic profile in the orbital angular velocity—is a direct consequence of frame dragging coupled with strong-field gravity in Kerr black holes. This naturally leads to a fundamental question: Is this behavior unique to rotating black holes, or can static black holes—devoid of intrinsic spin and hence lacking frame dragging—reproduce similar non-monotonic features, albeit through

a different mechanism?

In response to this question, we argued in our previous work that while static black holes lack rotational effects, they retain strong gravitational curvature. Consequently, the emergence of a non-monotonic angular velocity profile depends on identifying a surrogate mechanism that replicates the dynamical role of frame dragging. We proposed that this surrogate is the appearance of a stable gravitational potential minimum—either local or global—outside the event horizon, typically associated with a stable photon sphere [14].

Historically, such “minimum-maximum” potential pairs have been well documented in horizonless ultra-compact gravitational configurations, such that it can be stated with reasonable accuracy that most ultracompact gravitational models in the form of naked singularities exhibit stable photon spheres[15–17]. However, when the Weak Cosmic Censorship Conjecture (WCCC) is enforced, introducing an event horizon converts these models into legitimate black holes. In most cases, the previously accessible minimum gets hidden behind the horizon, resulting in purely monotonic velocity profiles. Nevertheless, there are models wherein despite the presence of an event horizon, a stable potential minimum persists in the exterior geometry. In such cases, the orbital angular velocity profile exhibits pronounced non-monotonic behavior, centered around this minimum [18, 19]. One such example, demonstrated in our earlier research[14], involves a black hole model constructed within a hybrid framework combining Gauss–Bonnet corrections and Massive Gravity. Encouraged by similar findings in another Massive Gravity formulation [19], we hypothesized that a broad class of black hole geometries within Massive Gravity may serve as viable candidates for exhibiting Aschenbach-like behavior.

To test this hypothesis, we consider three distinct black hole models in Massive Gravity and investigate the conditions under which this phenomenon may arise. Given that the existence and characteristics of potential extrema (such as photon spheres) are highly sensitive to the model’s parametric configuration, our approach entails:

An initial classification of generic black hole traits (existence of event horizons, photon spheres, and TCO behavior),
 Followed by a targeted analysis of whether the angular velocity profile develops a non-monotonic signature indicative of the Aschenbach-like effect.

It is important to stress that while a change in the angular velocity profile is the common observable across both rotating and static configurations, the underlying mechanisms are fundamentally different:

In rotating (Kerr) black holes, the Aschenbach effect stems from the interplay between frame dragging and strong gravity. In static black holes, the analogous behavior is induced through the formation of an exterior gravitational potential minimum, absent frame dragging.

Therefore, although the observational manifestations may resemble one another, the governing physics diverge substantially. This distinction in static models leads us to call this phenomenon in static black holes the Aschenbach-like effect instead of the Aschenbach effect.

II. METHODOLOGY

In this Article, for the analysis of photon spheres, we adopt the topological charge-based and approach, which has been thoroughly detailed in [20, 21] and our previous works [15, 16]. In the interest of brevity and to avoid redundancy, we do not revisit the foundational concepts here.

Also, in examining TCOs, we rely on the orbital relations and stability criteria formulated in studies [22–24]. Given the comprehensive nature of these references, we direct interested readers to those publications for an in-depth treatment of the methodology.

A. Topological Photon Sphere

To study the photonic sphere, we first need an effective potential. We use the effective potential that was constructed for the study of the topological method based on the metric coefficients of a spherically symmetric four-dimensional model. we have [20, 21]:

$$ds^2 = -dt^2 f(r) + \frac{dr^2}{g(r)} + \left(d\theta^2 + d\varphi^2 \sin^2(\theta)\right) h(r) = dr^2 g_{rr} - dt^2 g_{tt} + d\theta^2 g_{\theta\theta} + d\varphi^2 g_{\varphi\varphi}, \quad (1)$$

$$H(r, \theta) = \sqrt{\frac{-g_{tt}}{g_{\varphi\varphi}}} = \frac{1}{\sin \theta} \left(\frac{f(r)}{h(r)}\right)^{1/2}. \quad (2)$$

Now, to determine the charges and topological behavior of the model, we will first need a vector field using the effective potential H . For this purpose, we consider a general two dimensional vector field as ϕ which can be decomposed into two

components, ϕ^r and ϕ^Θ [20, 21],

$$\phi = (\phi^r, \phi^\Theta), \quad (3)$$

This vector field can be rewrite as $\phi = \|\phi\|e^{i\Theta}$, where $\|\phi\| = \sqrt{\phi \cdot \phi}$. Accordingly, the normalized vector can be defined as,

$$n^\iota = \frac{\phi^\iota}{\|\phi\|}, \quad (4)$$

where $\iota = 1, 2$ and $(\phi^1 = \phi^r)$, $(\phi^2 = \phi^\Theta)$. In terms of H , the vector field $\phi = (\phi^r, \phi^\Theta)$ can be written as follows:

$$\begin{aligned} \phi^r &= \frac{\partial_r H}{\sqrt{g_{rr}}} = \sqrt{g(r)} \partial_r H, \\ \phi^\Theta &= \frac{\partial_\theta H}{\sqrt{g_{\theta\theta}}} = \frac{\partial_\theta H}{\sqrt{h(r)}}. \end{aligned} \quad (5)$$

By employing the previously established relations and the definition of topological charge, one can systematically assign a charge to each photon sphere present in the spacetime [15, 16, 21]. Before drawing broader conclusions from this section, it is important to underscore a key finding from our earlier publications: In configurations where the model exhibits black hole characteristics, typically satisfying the condition of possessing an event horizon, one often finds a single unstable photon sphere located outside the horizon, characterized by a net topological charge of -1 . From the perspective of the effective potential, this corresponds to the presence of at least one maximum outside the horizon. Conversely, in horizonless configurations (i.e., naked singularities), the geometry commonly features not only an unstable photon sphere with a topological charge of -1 , but also one or two stable photon spheres with topological charges of $+1$. These are identified as local minima of the potential structure and represent dynamically stable light rings. These distinctions are of fundamental importance and will be revisited in subsequent discussions, particularly when analyzing the relationship between topological photon sphere and orbital dynamics in strongly curved spacetimes.

B. Time-like Circular Orbits (TCOs)

The geodesic behavior in any gravitational model is profoundly shaped by the form of the effective potential, derived from the interplay of fields within the model's action. These geodesics may either lack recognizable turning points or exhibit them, forming closed trajectories. In the case of null geodesics, such closed paths correspond to photon spheres, whereas in timelike geodesics, they manifest as TCOs. Both types of orbits may be either stable or unstable, depending on the curvature and potential landscape of the spacetime. In this study, we adopt a static, axisymmetric spacetime with an imposed \mathbb{Z}_2 symmetry under a (1+3) dimensional framework. This symmetry structure ensures that focusing the analysis on the equatorial plane does not compromise the generality of our results. Based on the metric equation—namely Eq. (1)—we consider the following key quantities [22]:

$$A = g_{\varphi\varphi}E^2 + g_{tt}L^2, \quad (6)$$

$$B = -g_{\varphi\varphi}g_{tt}, \quad (7)$$

which E and L are the energy and the angular momentum respectively. Now the Lagrangian can be recast as:

$$2\mathfrak{L} = -\frac{A}{B} = \varrho, \quad (8)$$

where $\varrho = -1, 0$ for time-like and null geodesics, respectively. Using the above Lagrangian, the effective potential can be rewritten as follows:

$$V_{\text{eff}(\varrho)}(r) = \varrho + \frac{A}{B}. \quad (9)$$

The concept of angular velocity (as measured by an observer at infinity) and β in terms of metric parameters [22].

$$\Omega = \frac{g_{tt}L}{g_{\varphi\varphi}E}, \quad (10)$$

$$\beta = -r^2\Omega^2 + f(r), \quad (11)$$

An important aspect to consider in the study of TCOs is the value of the β function. In regions where β is negative, the energy and angular momentum become imaginary, rendering these areas effectively forbidden for the presence of TCOs. Interested readers seeking a deeper understanding of these relationships, and more examples, are encouraged to refer to [22–24].

III. BLACK HOLES IN MASSIVE GRAVITY: ADVANTAGES AND DISADVANTAGES

The concept of a massive graviton originated with Markus Fierz and Wolfgang Pauli. They formulated a linear theory (Fierz-Pauli theory) describing a massive spin-2 particle in flat spacetime [25, 26]. However, this theory suffered from the van Dam-Veltman-Zakharov (vDVZ) discontinuity [25, 27]: predictions didn't smoothly reduce to General Relativity (GR) as the graviton mass approached zero, conflicting with precise solar system tests [25, 28]. Vainshtein proposed a resolution. He demonstrated that nonlinear interactions in massive gravity lead to strong effects ("Vainshtein screening") near massive sources, dynamically suppressing the helicity-0 mode of the graviton and restoring agreement with General Relativity (GR) in the massless limit, despite a finite graviton mass. This mechanism resolved the van Dam-Veltman-Zakharov (vDVZ) discontinuity by showing that linearized approximations break down in strong-field regimes, such as solar system scales. However, a consistent nonlinear completion of massive gravity—free of the Boulware-Deser ghost instability—was only achieved decades later by de Rham, Gabadadze, and Tolley (dRGT theory, 2010) [29], which explicitly incorporates Vainshtein screening as a core feature. Constructing a consistent, ghost-free nonlinear massive gravity theory proved challenging for decades due to the emergence of Boulware-Deser ghosts (unphysical negative-energy states) in early formulations. The field was revolutionized in 2010 by Claudia de Rham, Gregory Gabadadze, and Andrew Tolley (dRGT massive gravity). They identified a specific class of nonlinear interaction terms—tuned potential terms constructed from invariants of the dynamical metric and the fixed reference metric—which systematically eliminate the Boulware-Deser ghost to all orders in the Hamiltonian formulation. This provided the first consistent four-dimensional (4D), Lorentz-invariant theory of massive gravity in flat spacetime, free of the instability that had plagued earlier attempts. The theory relies on a reference metric (often Minkowski) and a carefully tuned structure of potential terms to preserve constraints that eliminate the ghost. Subsequent analyses by S.F. Hassan and R.A. Rosen confirmed the absence of the Boulware-Deser ghost in dRGT through a canonical ADM formalism [29, 30].

Shortly after the dRGT formulation, intense research began to find black hole solutions:

- ♣ **Schwarzschild-like Solutions:** Early solutions assumed specific symmetries or ansatzes, often recovering the standard Schwarzschild metric but with the graviton mass parameters appearing as effective cosmological constants or influencing asymptotic behavior differently than in GR.

- ♣ **Hairy Black Holes:** It became clear that dRGT massive gravity allows for black holes with "hair" – additional parameters beyond mass, charge, and angular momentum, forbidden in GR by no-hair theorems. These hairs are directly related to the graviton mass parameters and the structure of the potential. Spherically symmetric solutions often involve additional fields (Stückelberg fields) or manifest as modifications to the metric components.

- ♣ **Bimetric Gravity:** A closely related and dynamically richer framework involves two interacting metrics: one dynamical (spacetime) and one fixed reference metric (often Minkowski or de Sitter). Bimetric gravity naturally incorporates massive gravity limits and provides a more flexible setting for finding black hole solutions, including rotating ones (analogues of Kerr) which are much harder to find in pure dRGT [30, 31].

Although the formation of a black hole in the form of Massive gravity still follows the same basic principles of general relativity, but Massive gravity modifies how gravity works. The key differences lie in how the collapse proceeds and the resulting structure of the black hole due to the modified gravitational dynamics, means:

1. Modified Field Equations:

Einstein's equations are replaced by equations where the graviton mass terms act as an effective source of stress-energy:

$$G_{\mu\nu} = 8\pi GT_{\mu\nu}(\text{matter}) + T_{\mu\nu}(\text{mass}).$$

This $T_{\mu\nu}(\text{mass})$ depends non-trivially on the metric and the reference/Stückelberg fields.

2. Altered Dynamics:

The mass terms suppress gravitational fluctuations at large distances (Yukawa-like decay), change the propagation speed of gravity waves, and introduce new degrees of freedom. This affects the collapse process and the equilibrium configurations.

3. Vainshtein Mechanism:

The Vainshtein mechanism is a nonlinear screening effect that dynamically suppresses the extra degrees of freedom (the 5 polarizations of the massive graviton) and the deviations from General Relativity in regions of strong gravity or high matter density. Near the collapsing object and the resulting black hole, the Vainshtein mechanism is active and making the gravitational field look very similar to General Relativity close to the horizon, while deviations become significant at larger

distances (asymptotics).

4. "Hair" Formation:

The requirement to satisfy the modified field equations and boundary conditions, often involving the Stückelberg fields or the interplay with the reference metric, necessitates additional parameters "hair" beyond mass, charge, and angular momentum to fully characterize the black hole.

In summary:

Black holes in massive gravity are a direct consequence of gravitational collapse within a modified theory where the graviton has mass. The graviton mass terms can act as an effective dark energy driving the late-time accelerated expansion of the universe without needing a cosmological constant or quintessence fields. Driven by the resolution of the ghost problem (dRGT theory), they represent a vibrant research area.

Their key features are modified asymptotics, the potential for "hair," and the influence of the Vainshtein mechanism near the horizon.

Their Advantages include potential explanations for dark energy/dark matter, singularity resolution ¹, and unique observational signatures.

However, significant disadvantages persist: theoretical complexity, stability concerns, stringent constraints from gravitational wave astronomy, causality and superluminality ² and naturalness ³ issues.

A. Bardeen AdS Black Holes in Massive Gravity

In the presence of massive gravity, the action coupled to nonlinear electrodynamics with negative cosmological constant is given by [32]:

$$S = \frac{1}{2} \int d^4x \sqrt{-g} \left[R - 2\Lambda + m_g^2 \sum_i^4 c_i \mathcal{U}_i(g, f) - \frac{1}{4\pi} \mathcal{L}(F) \right], \quad (12)$$

where R, Λ , m_g and f are scalar curvature, cosmological constant, parameter of massive gravity and symmetric tensor respectively, c_i are constants and \mathcal{U}_i are polynomials of eigenvalues of the (4×4) matrix $\mathcal{K}_\nu^\mu = \sqrt{g^{\mu\alpha} f_{\alpha\nu}}$ which can be written as:

$$\begin{cases} \mathcal{U}_1 = [\mathcal{K}], \\ \mathcal{U}_2 = [\mathcal{K}]^2 - [\mathcal{K}^2], \\ \mathcal{U}_3 = [\mathcal{K}]^3 - 3[\mathcal{K}][\mathcal{K}^2] + 2[\mathcal{K}^3], \\ \mathcal{U}_4 = [\mathcal{K}]^4 - 6[\mathcal{K}^2][\mathcal{K}]^2 + 8[\mathcal{K}^3][\mathcal{K}] + 3[\mathcal{K}^2]^2 - 6[\mathcal{K}^4]. \end{cases}$$

$$\mathcal{L}(F) = \frac{1}{2se^2} \left(\frac{\sqrt{2e^2 F}}{1 + \sqrt{2e^2 F}} \right)^{\frac{5}{2}},$$

with $[\mathcal{K}] = [\mathcal{K}_\mu^\mu]$ and $\mathcal{L}(F)$ a function of $F \equiv \frac{1}{4} F_{\mu\nu} F^{\mu\nu}$ is the Lagrangian density of Bardeen source [33].

The spherically-symmetric static metric line element of such a spacetime is given by the following [34]:

$$f(r) = 1 - \frac{2Mr^2}{(r^2 + q^2)^{\frac{3}{2}}} + \frac{r^2}{l^2} + m_g^2 \left(C^2 c_2 + \frac{C c_1 r}{2} \right), \quad (13)$$

where M , l and q are mass, AdS radius and magnetic charge.

As stated in the past, since the behavior of black holes in a massive gravitational structure is deeply dependent on parameter values, it is first useful to consider the effect of changes in each parameter on the radius of the event horizon.

¹ Some solutions in massive gravity exhibit regular black holes or horizons without singularities. The effective stress-energy from the mass terms can violate energy conditions, potentially halting collapse before a singularity forms. This could resolve the central singularity problem of GR

² Some solutions exhibit apparent superluminal propagation of fluctuations around the background solution

³ Explaining the extremely small graviton mass required by observations (if non-zero) is challenging from a particle physics perspective

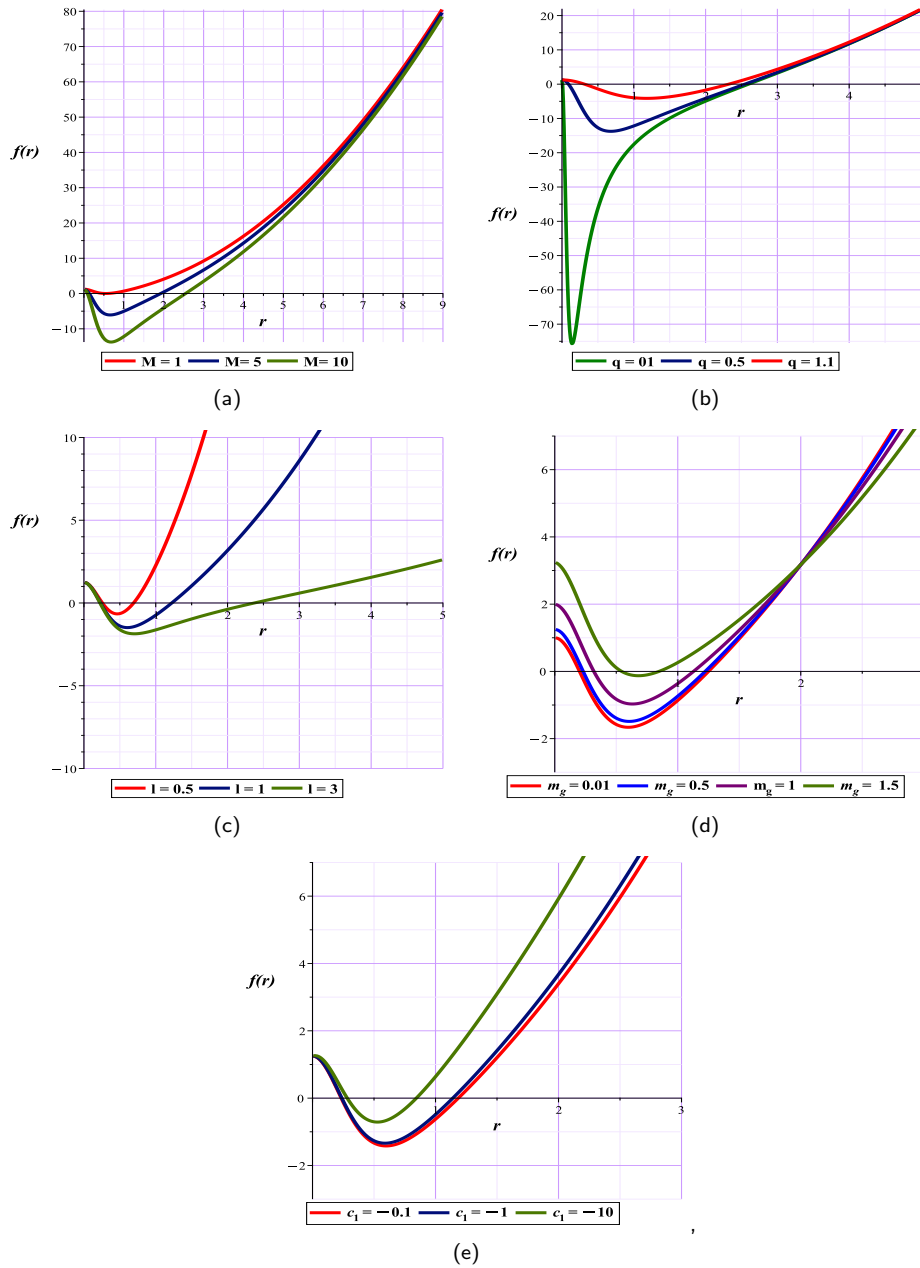


FIG. 1. Metric function Fig (1a): With $l = 1, q = 0.5, C = 1, c_1 = -1, c_2 = 1, m_g = 0.5$ with different M , (1b): With $l = 1, M = 10, C = 1, c_1 = -1, c_2 = 1, m_g = 0.5$ with different q (1c): With $M = 2, q = 0.5, C = 1, c_1 = -1, c_2 = 1, m_g = 0.5$ with different l (1d): With $M = 2, l = 1, q = 0.5, C = 1, c_1 = -1, c_2 = 1$ with different m_g (1e): With $M = 2, l = 1, q = 0.5, C = 1, c_2 = 1, m_g = 0.5$ with different c_1 for Bardeen black holes in massive gravity

The behavioral differences of the metric function, driven by parametric variations, are clearly observable in Fig. (1). As evident from panels Fig. (1(a)) and Fig. (1(d)), the interplay between the black hole mass and the graviton mass significantly influences the structure of the solution. When these two masses approach one another in magnitude, the system tends toward a naked singularity regime, implying a breakdown of the event horizon. A similar trend is observed with increasing electric charge Fig. (1(b)): higher values of charge progressively push the system toward singular behavior, eliminating the possibility of horizon formation. Furthermore, increasing the curvature radius of the spacetime—alternatively interpreted as the AdS radius—directly affects the radius of the event horizon. As depicted in Fig. (1(c)), larger values of l expand the horizon radius; however, excessive growth (e.g., $l = 20$) leads to the degeneration of the metric function into a single-root structure, effectively eliminating the outer horizon. The influence of the parameter c_1 appears negligible within small domains. Nevertheless, beyond a critical threshold, its contribution becomes substantial, causing the Cauchy horizon

and the event horizon to approach one another Fig. (1(e)), which signals a reduction in the inter-horizon region.

In search of the Aschenbach-like phenomenon

Given the complexity of the model and the multitude of governing parameters, it is evident that an analytical solution is infeasible. As such, parameter initialization followed by numerical analysis is essential—an approach we were already compelled to adopt in our study of the metric function. To proceed toward detecting Aschenbach-like behavior, we now consider a baseline configuration by assigning the values $M = 2, l = 1, q = 0.5, C = 1, c_1 = -1, c_2 = 1, m_g = 0.5$ to the relevant parameters. This initial scenario serves as a reference point to investigate the emergence of non-monotonic angular velocity features under simplified but physically representative conditions. To ensure that the model under consideration truly exhibits black hole behavior, it is instructive to begin with an analysis of its general structural features. By numerically solving the metric function, we find that the spacetime possesses two distinct horizons:

- A Cauchy horizon at $r = 0.2306$,
- An event horizon at $r = 1.2232$.

This double-horizon structure satisfies the Weak Cosmic Censorship Conjecture (WCCC), confirming that any singularity remains hidden behind an event horizon. Furthermore, using the relations for mass:

$$M = \frac{(q^2 + r^2)^{\frac{3}{2}} (2C^2 l^2 c_2 m_g^2 + C l^2 r c_1 m_g^2 + 2l^2 + 2r^2)}{4r^2 l^2} \quad (14)$$

and temperature:

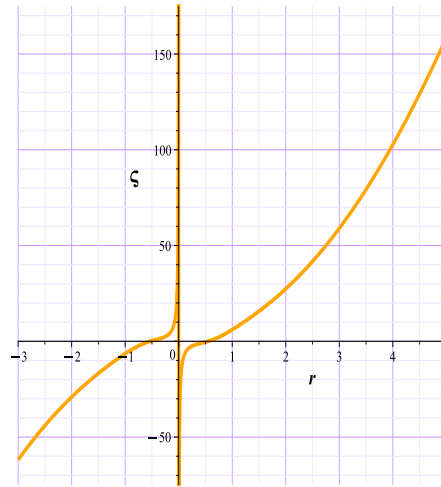
$$T = \frac{(2C r^3 c_1 m_g^2 + (2C^2 c_2 m_g^2 + 2) r^2 - C q^2 r c_1 m_g^2 - 4q^2 (C^2 c_2 m_g^2 + 1)) l^2 + 6r^4}{8r l^2 (q^2 + r^2) \pi} \quad (15)$$

we can compute the heat capacity of the model via below Equation.

$$\varsigma = \left. \frac{\partial M}{\partial T} \right|_{r_h} = \left(\frac{\partial M}{\partial r} \right)_{r_h} \left(\frac{\partial r}{\partial T} \right)_{r_h}. \quad (16)$$

The local thermodynamic stability of a black hole is typically assessed by examining the behavior of its heat capacity:

- A positive heat capacity corresponds to thermodynamic stability.
- A negative heat capacity indicates instability, as established in the literature [35–37].



(a)

FIG. 2. The heat capacity with $M = 2, l = 1, q = 0.5, C = 1, c_1 = -1, c_2 = 1, m_g = 0.5$ for Bardeen black holes in massive gravity

By plotting the heat capacity equation with respect to the chosen parametric values Fig. (2), we clearly observe thermodynamically stable behavior for the model within the investigated regime. This analysis reinforces the black hole nature of the configuration and lays the foundation for studying phenomena such as non-monotonic angular velocity profile in the context of Aschenbach-like effects. We now turn to its geodesic behavior of the model. As previously noted,

by examining the general form of the metric function as outlined in Eq. (1), one can predict two distinct regimes for characteristic behaviors of TCOs based on the stability of the photon sphere:

1) For radial values $r < r_{\text{PS}}$, the quantity β becomes negative, indicating that TCOs are forbidden in this domain. Consequently, the allowed spatial region for TCOs is restricted to radii $r > r_{\text{PS}}$.

2) In contrast, for $r > r_{\text{PS}}$, a negative β similarly prohibits the existence of TCOs. Here, TCOs are confined to the interior region with radii $r < r_{\text{PS}}$. This geometric restriction reflects the causal and dynamical influence of the photon sphere on the surrounding geodesic structure. The sign and behavior of β act as a discriminant for admissible orbital zones and play a crucial role in shaping the morphology of accretion disks and observational features such as photon rings and ISCO-related dynamic.

Considering the Eq. (2) and Eq. (5) we obtain the effective potential H and components of the vector field $\phi(r, \theta)$ as:

$$H = \frac{\sqrt{1 - \frac{2r^2 M}{(q^2 + r^2)^{\frac{3}{2}}} + \frac{r^2}{l^2} + \left(\frac{1}{2}rc_1 C + C^2 c_2\right) m_g^2}}{\sin(\theta) r}, \quad (17)$$

$$\phi^{r_h} = -\frac{\left((c_2 m_g^2 C^2 + \frac{1}{4}rc_1 m_g^2 C + 1)(q^2 + r^2)^{\frac{5}{2}} - 3M r^4\right) \csc(\theta)}{(q^2 + r^2)^{\frac{5}{2}} r^2}, \quad (18)$$

$$\phi^\Theta = -\frac{\sqrt{\frac{\left((c_2 m_g^2 C^2 + \frac{1}{2}rc_1 m_g^2 C + 1)l^2 + r^2\right)(q^2 + r^2)^{\frac{3}{2}} - 2r^2 M l^2}{(q^2 + r^2)^{\frac{3}{2}} l^2}} \cot(\theta) \csc(\theta)}{r^2}. \quad (19)$$

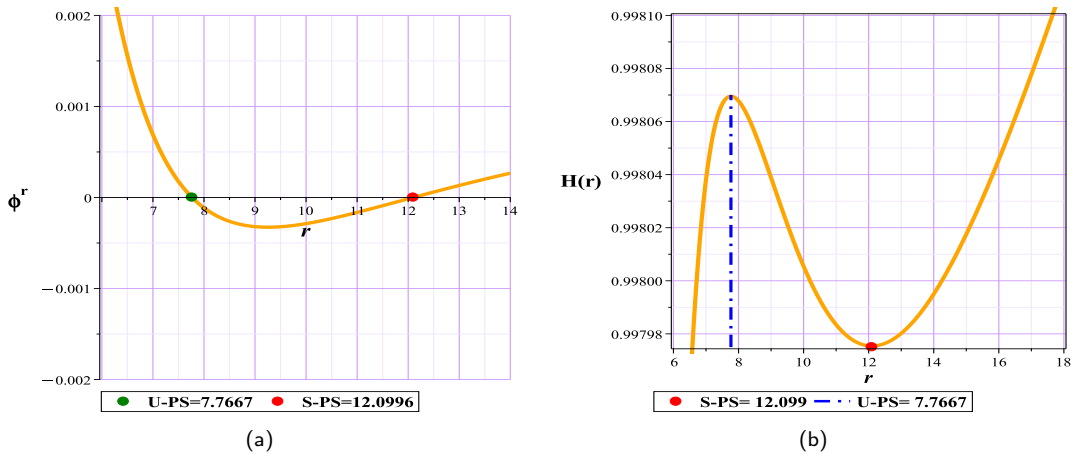


FIG. 3. Fig (3a): The photon spheres location at $(r, \theta) = (7.7667, 1.57)$ and $(r, \theta) = (12.0996, 1.57)$ with respect to $M = 2, l = 1, q = 0.5, C = 1, c_1 = -1, c_2 = 1, m_g = 0.5$ in the $(r - \theta)$ plane of the normal vector field n , (3b): the topological potential $H(r)$ for Bardeen black holes in massive gravity

As illustrated in Fig. (3), while the model indeed exhibits black hole behavior, a notable feature emerges: two distinct photon spheres—an unstable photon sphere (U-PS:corresponding to a maximum of the potential H) and a stable photon sphere (S-PS:associated with a local minimum of H)—both appear outside the event horizon. Now, if we look at the beta function for this case Fig. (4(a)), we will see that, as mentioned, the region between these two photon spheres has positive beta, and outside it, as stated in the two conditions above, there are forbidden regions due to the negative beta.

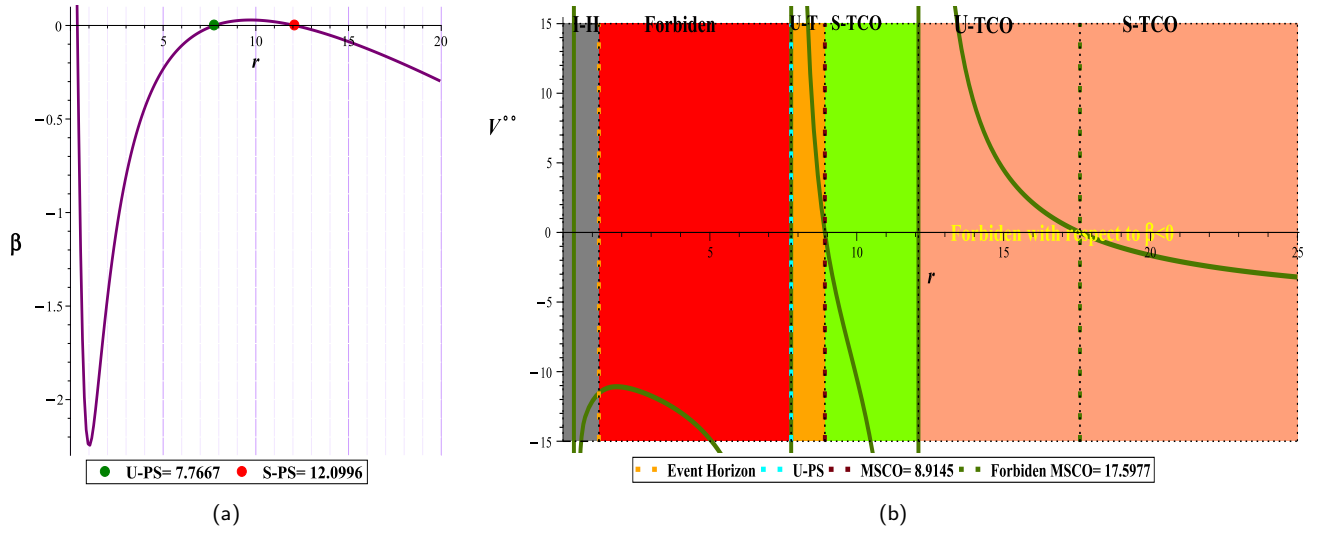


FIG. 4. Fig (4a): β diagram (4b):MSCO localization and space classification for the Bardeen black holes in massive gravity

In Fig. (4(b)), For potential V , as defined by Eq. (9) we plot the second derivative of the V , to investigate the geodesic behavior of spacetime surrounding the black hole. The profile reveals the presence of two marginally stable circular orbits (MSCOs) :

- The first MSCO, located within the physically admissible domain, marks the transition between stable and unstable TCOs. Its presence serves as the boundary for geodesic stability in orbital motion. This structure creates a geodesically bounded region between the two photon spheres where stable circular motion is allowed—a behavior that strongly correlates with the conditions necessary for the emergence of Aschenbach-like profiles in the angular velocity.
- The second MSCO, although mathematically identifiable as a transitional point between two distinct orbital regimes, resides in a region where the function β becomes negative. Since negative β implies imaginary energy or angular momentum for test particles, this zone lacks physical legitimacy and is classified as a forbidden region .

Having established the theoretical framework, physical prerequisites, and resulting conditions, we now turn our attention to the angular velocity profile and examine its behavior within the scope of this model. In our previous work, we thoroughly explored the mechanism underlying the emergence of this phenomenon in static black hole configurations, highlighting the dependencies of angular velocity on several interconnected quantities:

- Energy and angular momentum,
- The form of the metric function,
- The behavior of the β parameter, which governs geodesic admissibility.

$$\begin{aligned}
 \Omega &= \frac{Lf}{Er^2}, \\
 E &= \frac{f}{\sqrt{\beta}}, \\
 L &= -\frac{r^2\Omega}{\sqrt{\beta}}, \\
 \Omega &= \sqrt{\frac{f(r) - \beta}{r^2}}.
 \end{aligned} \tag{20}$$

This multi-variable interdependence implies that deviations from monotonicity in the angular velocity are not merely geometric artifacts, but rather stem from a delicate balance between metric structure and dynamical constraints.

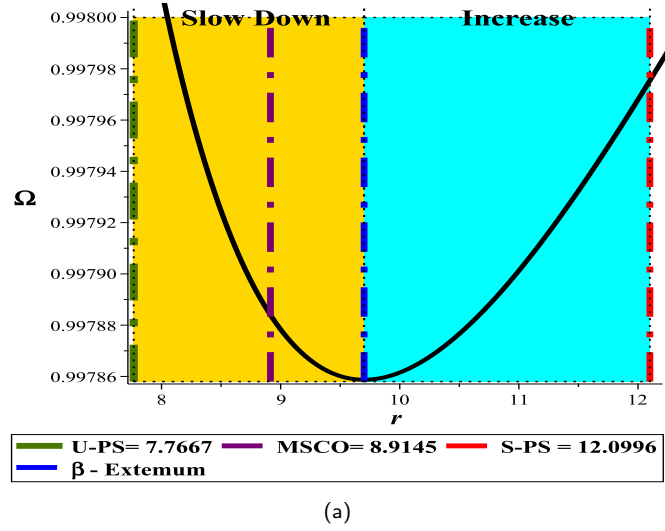


FIG. 5. Angular velocity VS r with $M = 2, l = 1, q = 0.5, C = 1, c_1 = -1, c_2 = 1, m_g = 0.5$ for the Bardeen black holes in massive gravity

As illustrated in Fig. (5), the angular velocity exhibits a decreasing trend along unstable TCOs originating from the edge of the unstable photon sphere—a behavior that aligns with theoretical expectations.

However, notably, this monotonic decline does not persist indefinitely. Upon approaching the minimum of the β function at $r = 9.7006$, and continuing toward the stable photon sphere—which structurally coincides with a local minimum in the effective potential—the angular velocity begins to increase, giving rise to a globally non-monotonic profile. This reversal in slope is precisely the type of behavior we aimed to identify as indicative of Aschenbach-like dynamics.

A particularly intriguing feature visible in the figure is that the angular velocity's decreasing trend does not coincide with the location of the MSCO. Moreover, even some stable TCOs appear to experience a reduction in angular velocity, suggesting that the inflection point of the profile is governed more by the underlying spacetime geometry—particularly the structure of the effective potential and the behavior of β —than by traditional orbital stability criteria.

This detection strengthens the argument that in the absence of rotational frame-dragging, the emergence of non-monotonicity in angular velocity can still arise due to spacetime curvature alone, provided the geometry allows for appropriate potential extrema. Consequently, the present model, now confirmed to host both a stable photon sphere and geodesically bounded orbital zones outside the event horizon, is an ideal candidate for detecting Aschenbach-like behavior within a non-rotating framework.

B. Non-linear charged AdS black hole in massive gravity

If we use the following Lagrangian instead of the Bardeen Lagrangian in Eq. (12),

$$\mathcal{L}(F) = F e^{-\frac{k}{2Q}} (2Q^2 F)^{\frac{1}{4}},$$

we will arrive at a nonlinear charged AdS model in massive gravity with metric of the spacetime as follows [38]:

$$f(r) = 1 - \frac{2M}{r} e^{-\frac{k}{2r}} + \frac{r^2}{l^2} + m_g^2 \left(\frac{C c_1 r}{2} + C^2 c_2 \right), \quad (21)$$

where k is a fixed characteristic parameter of the non-linear electrodynamics by which the charge Q and the mass M of the system are related as $Q^2 = Mk$.

Given that the methodology and analytical framework have been thoroughly outlined in preceding sections, and considering the recurring structure of the study, we will refrain from repeating detailed procedural explanations in the remainder of this work. To maintain clarity and avoid unnecessary fatigue or confusion, from this point onward, we shall focus exclusively on presenting essential findings and critical observations relevant to each parametric scenario.

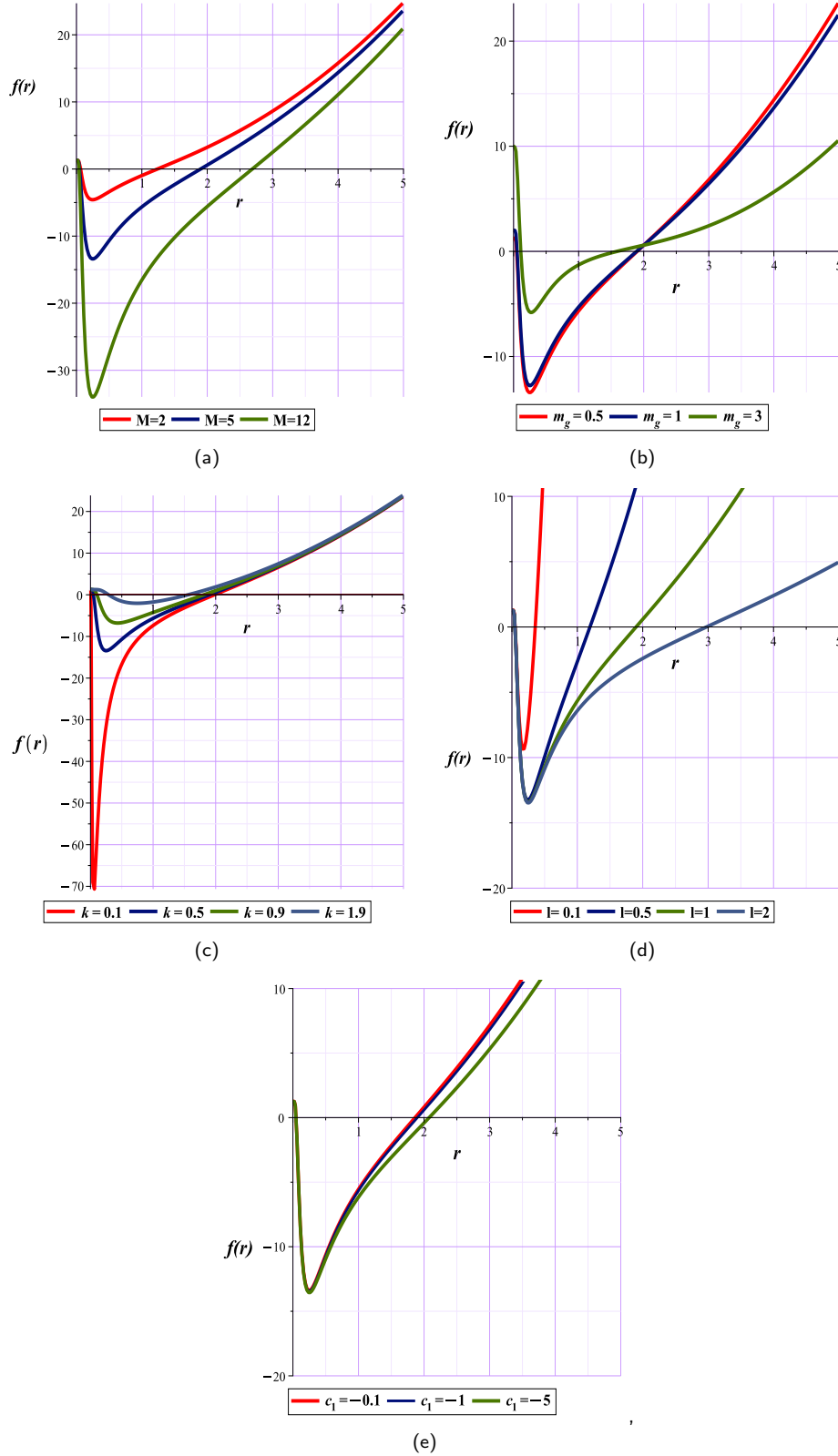


FIG. 6. Metric function Fig (1a): With $l = 1, k = 0.5, C = 1, c_1 = -1, c_2 = 1, m_g = 0.53$ with different M , (1b): With $M = 5, l = 1, k = 0.5, C = 1, c_1 = -1, c_2 = 1$ with different m_g (1c): With $M = 5, l = 1, C = 1, c_1 = -1, c_2 = 1, m_g = 0.5$, with different k (1d): With $M = 5, k = 0.5, C = 1, c_1 = -1, c_2 = 1, m_g = 0.5$ with different l (1e): With $M = 5, l = 1, k = 0.5, C = 1, c_2 = 1, m_g = 0.5$ with different c_1 for Non-linear charged AdS black hole in massive gravity

The behavioral differences of the metric function, driven by parametric variations, are clearly observable in Fig. (6). It can be clearly seen that while changing l and c_1 does not have a particular effect in terms of metric and geometric horizon, increasing k causes the model to move towards extremality.

In search of the Aschenbach-like phenomenon

To proceed toward detecting Aschenbach-like behavior, we now consider a baseline configuration by assigning the values $M = 2, l = 1, k = 0.5, C = 1, c_1 = -1, c_2 = 1, m_g = 0.53$ to the relevant parameters. By numerically solving the metric function, we find that the spacetime possesses two distinct horizons:

- A Cauchy horizon at $r = 0.0643$,
- An event horizon at $r = 1.2381$.

Now with respect to Eq. (2) and Eq. (5) for the effective potential H and components of the vector field $\phi(r, \Theta)$ we have:

$$H = \frac{\sqrt{1 - \frac{2e^{-\frac{k}{2r}}M}{r} + \frac{r^2}{l^2} + \left(\frac{rc_1}{2} + Cc_2\right) Cm_g^2}}{\sin(\theta) r}, \quad (22)$$

$$\phi^{r_h} = -\frac{\left(\frac{M(k-6r)e^{-\frac{k}{2r}}}{2} + r^2 \left(c_2 m_g^2 C^2 + \frac{1}{4} r c_1 m_g^2 C + 1\right)\right) \csc(\theta)}{r^4}, \quad (23)$$

$$\phi^\Theta = -\frac{\sqrt{2} \sqrt{-4e^{-\frac{k}{2r}} M l^2 + 2r \left(c_2 m_g^2 C^2 + \frac{1}{2} r c_1 m_g^2 C + 1\right) l^2 + r^2}}{2r^2} \cot(\theta) \csc(\theta). \quad (24)$$

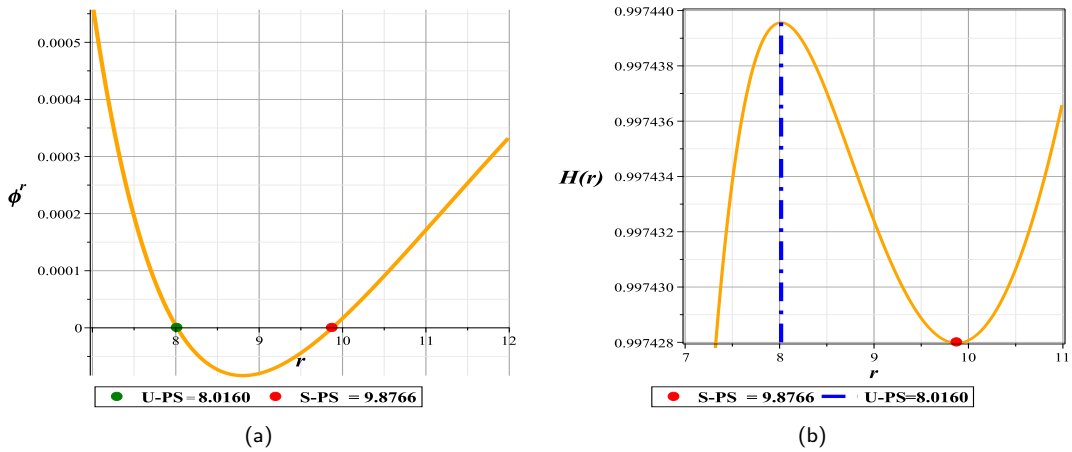


FIG. 7. Fig (7a): The photon spheres location at $(r, \theta) = (8.0160, 1.57)$ and $(r, \theta) = (9.8766, 1.57)$ with respect to $M = 2, l = 1, k = 0.5, C = 1, c_1 = -1, c_2 = 1, m_g = 0.53$ in the $(r - \theta)$ plane of the normal vector field n , (7b): the topological potential $H(r)$ for Non-linear charged AdS black hole in massive gravity

As can be seen in Fig. (7), for the selected parameters, a potential minimum and a maximum are still evident outside the event horizon, representing a stable sphere photon (red dot) and an unstable sphere photon (green dot) in the ϕ^r diagram.

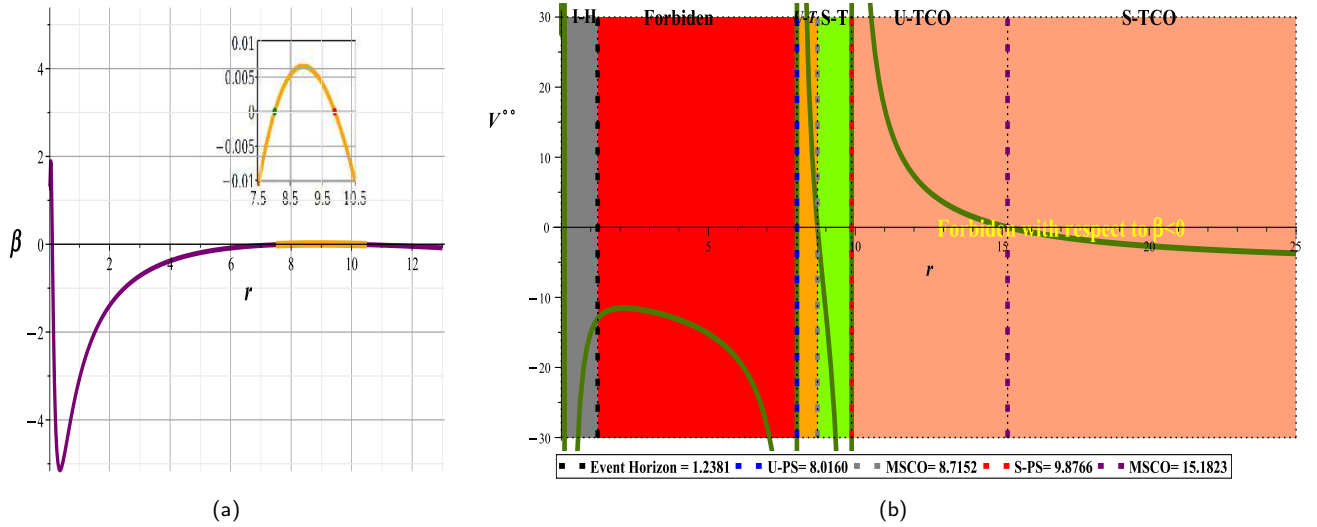


FIG. 8. Fig (4a): β diagram, $U - PS(\text{blue dot}) = 8.0160$ and $S - PS(\text{red dot}) = 9.8766$ (4b): MSCO localization and space classification for the Non-linear charged AdS black hole in massive gravity

In Fig. (8), we have plotted the second derivative for the potential V as it is evident. It can still be seen that there are two MSCOs, the first one is in the acceptable physical range and the second one is in the negative β region and is classified as a forbidden region.

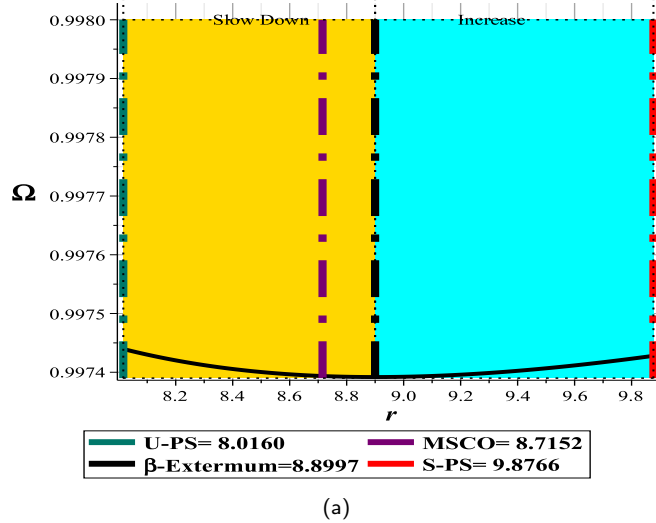


FIG. 9. Angular velocity VS r with $M = 2, l = 1, k = 0.5, C = 1, c_1 = -1, c_2 = 1, m_g = 0.53$ for the Non-linear charged AdS black hole in massive gravity

Similar to the previous model, as shown in Fig. (9), the angular velocity in this model, initially exhibits a decreasing trend along the time-like unstable circular orbits originating from the edge of the unstable photon sphere - a behavior that is in line with theoretical expectations. However, it is noteworthy that this uniform decrease does not continue indefinitely. Approaching the minimum β at $r = 8.8997$ and continuing towards the stable photon sphere - which structurally corresponds to a local minimum in the effective potential - the angular velocity starts to increase, leading to a globally non-uniform profile. This slope inversion is the hallmark of the Aschenbach-like phenomenon.

C. ModMax-dRGT-like Black hole in massive gravity

If we use the following Lagrangian in Eq. (12), we will arrive at a ModMax-dRGT-like Black hole in massive gravity with metric of the spacetime as follows [39]:

$$\mathcal{L}(\mathcal{F}) = \mathcal{S} \cosh \gamma - \sqrt{\mathcal{S}^2 + \mathcal{P}^2} \sinh \gamma, \quad (25)$$

$$f(r) = 1 - \frac{M}{r} - \frac{\Lambda}{3}r^2 + \frac{q^2 e^{-\gamma}}{r^2} + m_g^2 C \left(\frac{c_1 r}{2} + c_2 C \right), \quad (26)$$

where $\mathcal{S} = \frac{\mathcal{F}}{4}$ and $\mathcal{P} = \frac{\tilde{\mathcal{F}}}{4}$, respectively, are a true scalar, and a pseudoscalar and $\mathcal{F} = F_{\mu\nu}F^{\mu\nu}$ is the Maxwell invariant. Also Λ , is the cosmological constant, M and γ are mass and the dimensionless parameter (which is known as the ModMax's parameter).

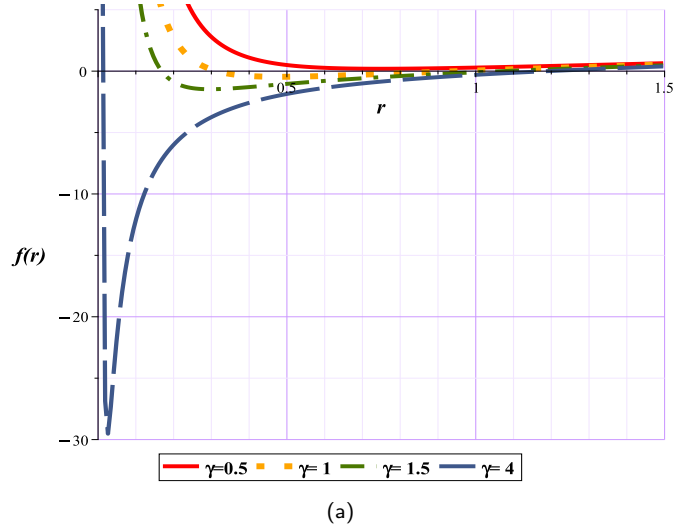


FIG. 10. Metric function Fig (1a): With $M = 1.5$, $\Lambda = -0.5$, $q = 1$, $C = 0.4$, $c_1 = -12$, $c_2 = 25$, $m_g = 0.1$ with different γ for ModMax-dRGT-like Black hole in massive gravity

As can be seen in Fig. (10), since in this model the γ parameter will have a significant effect on the gravitational behavior of the model, in such a way that small values (e.g. $\gamma < 0.6686$) will push the model towards extremalization and larger values will lead to black hole behavior, we therefore plot the metric function in two cases.

$$\mathbf{1.} (\gamma < 0.6686)$$

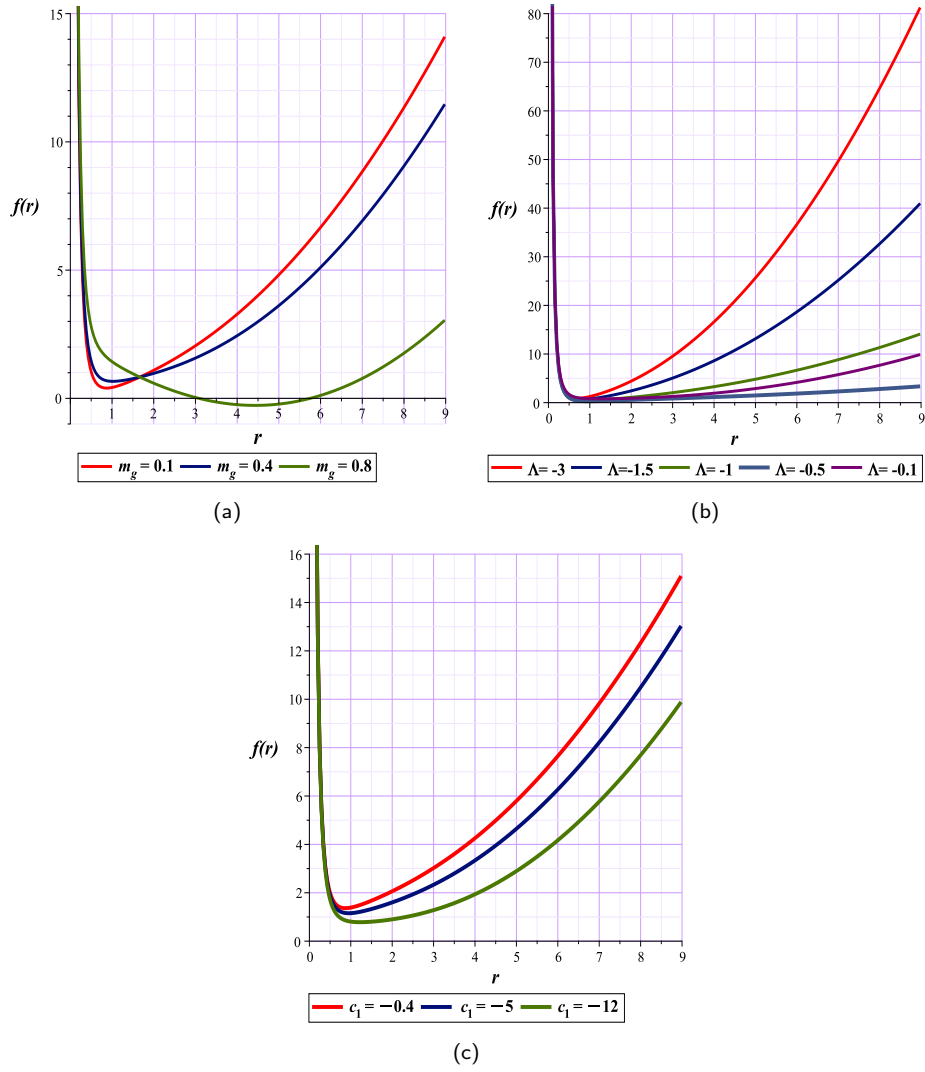


FIG. 11. Metric function Fig (11a): With $M = 1.5$, $\Lambda = -0.5$, $\gamma = 0.3$, $q = 1$, $C = 0.4$, $c_1 = -12$, $c_2 = 25$, with different m_g , (11b): With $M = 1.5$, $\gamma = 0.3$, $q = 1$, $C = 0.4$, $c_1 = -12$, $c_2 = 25$, $m_g = 0.5$ for different Λ (11c): With $M = 1.5$, $\Lambda = -0.5$, $\gamma = 0.3$, $q = 1$, $C = 0.4$, $c_2 = 25$, $m_g = 0.5$ with different c_1 for the ModMax-dRGT-like Black hole in massive gravity

As shown in Fig. (11), depending on the parametric choices, the structure exhibits black hole behavior only when the mass of the graviton component approaches the mass of the model. Otherwise, varying the parameters has practically no effect, leaving the model in a singularity state without a horizon.

$$2.(\gamma > 0.6686)$$

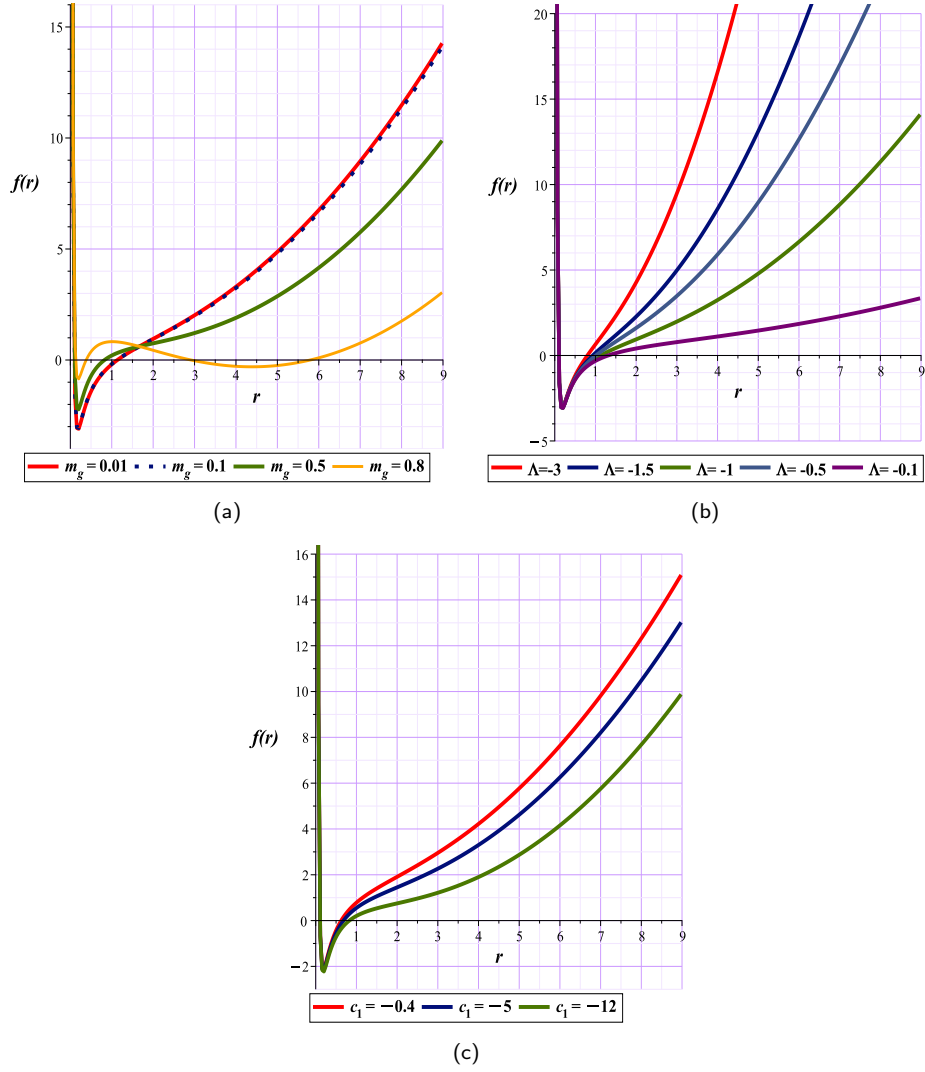


FIG. 12. Metric function Fig (12a): With $M = 1.5, \Lambda = -0.5, \gamma = 2, q = 1, C = 0.4, c_1 = -12, c_2 = 25$, with different m_g , (12b): With $M = 1.5, \gamma = 2, q = 1, C = 0.4, c_1 = -12, c_2 = 25, m_g = 0.1$ for different Λ (12c): With $M = 1.5, \Lambda = -0.5, \gamma = 2, q = 1, C = 0.4, c_2 = 25, m_g = 0.1$ with different c_1 for the ModMax-dRGT-like Black hole in massive gravity

In Fig. (12), we see that increasing the strength of the electromagnetic field (through increasing γ) with the same choice of parameters as before causes the behavior of the model to change completely, and it exhibits the event horizon and takes the form of a black hole. In Fig. (12a)), we can see that increasing the gravitational mass increases the number of horizons.

In search of the Aschenbach-like phenomenon

To proceed toward detecting Aschenbach-like behavior, we now consider a baseline configuration by assigning the values $M = 2, \Lambda = -0.5, \gamma = 2, q = 1, C = 0.4, c_1 = -12, c_2 = 25, m_g = 0.5$ to the relevant parameters. By numerically solving the metric function, we find that the spacetime possesses two distinct horizons:

- A Cauchy horizon at $r = 0.0728$,
- An event horizon at $r = 1.2531$.

Again, with considering the Eq. (2) and Eq. (5) we have:

$$H = \frac{\sqrt{9 - \frac{9M}{r} - 3r^2\Lambda + \frac{9q^2e^{-\gamma}}{r^2} + 9\left(\frac{rc_1}{2} + Cc_2\right)Cm_g^2}}{3\sin(\theta)r}, \quad (27)$$

$$\phi^{rh} = -\frac{\csc(\theta)(4C^2r^2c_2m_g^2 + Cr^3c_1m_g^2 + 8q^2e^{-\gamma} + 4r^2 - 6Mr)}{4r^4}, \quad (28)$$

$$\phi^\Theta = -\frac{\sqrt{6} \sqrt{\frac{3C r^3 c_1 m_g^2 - 2r^4 \Lambda + (6C^2 c_2 m_g^2 + 6)r^2 - 6Mr + 6q^2 e^{-\gamma}}{r^2}} \cot(\theta) \csc(\theta)}{6r^2}. \quad (29)$$

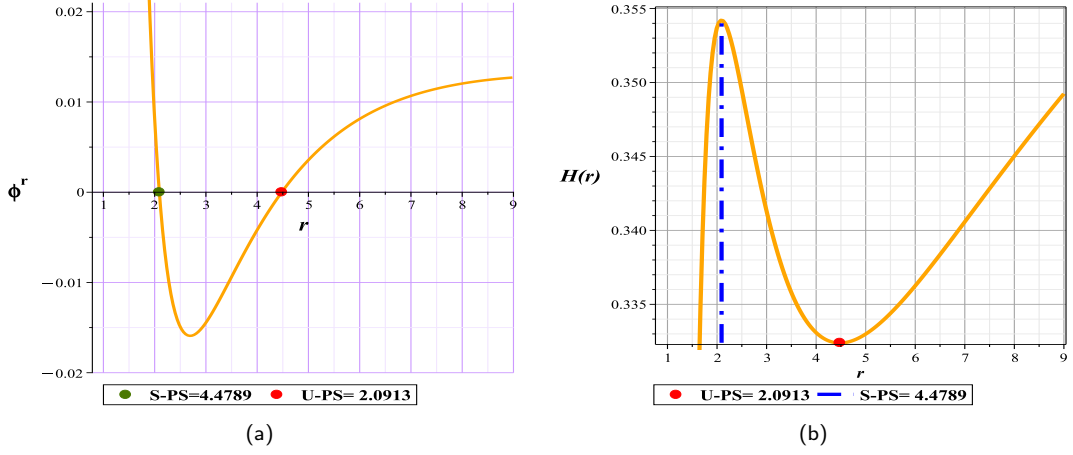


FIG. 13. Fig (13a): The photon spheres location at $(r, \theta) = (2.0913, 1.57)$ and $(r, \theta) = (4.4789, 1.57)$ with respect to $M = 2, \Lambda = -0.5, \gamma = 2, q = 1, C = 0.4, c_1 = -12, c_2 = 25, m_g = 0.5$ in the $(r - \theta)$ plane of the normal vector field n , (13b): the topological potential $H(r)$ for the ModMax-dRGT-like Black hole in massive gravity

For the selected parameters, a potential extremums are still evident outside the event horizon, representing a stable sphere photon (red dot) and an unstable sphere photon (green dot) in the ϕ^r diagram, see Fig. (13).

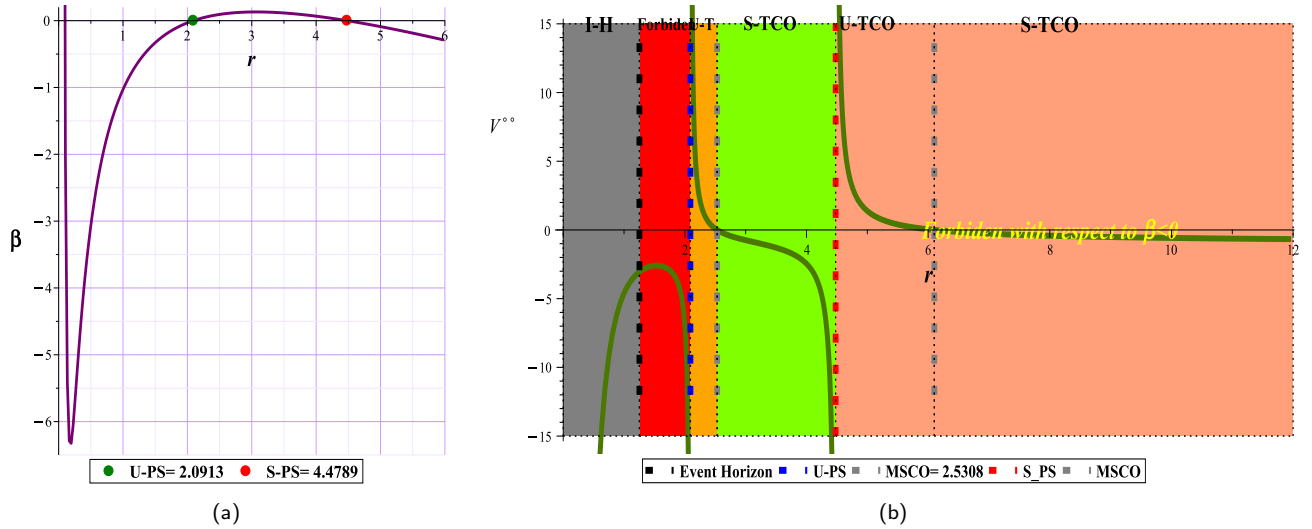


FIG. 14. Fig (14a): β diagram (14b):MSCO localization and space classification for the ModMax-dRGT-like Black hole in massive gravity

As it is evident in Fig. (14), for the second derivative of potential V there are two MSCOs. The first one is in the acceptable physical range and the second one is in the negative β region and is classified as a forbidden region.

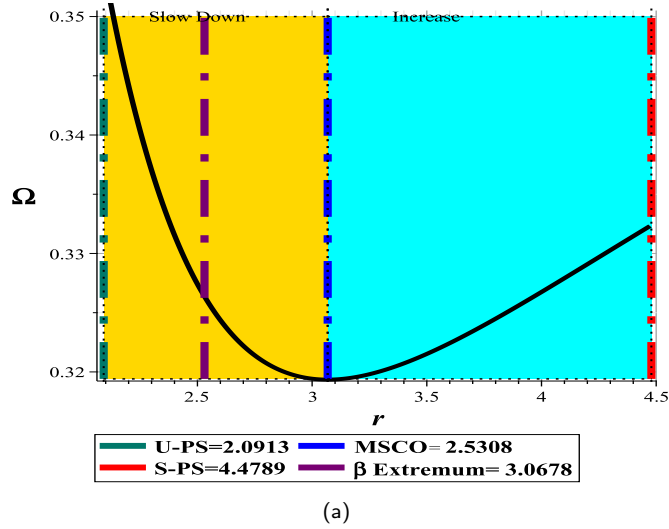


FIG. 15. Angular velocity VS r with $M = 2$, $\Lambda = -0.5$, $\gamma = 2$, $q = 1$, $C = 0.4$, $c_1 = -12$, $c_2 = 25$, $m_g = 0.5$ for the ModMax-dRGT-like Black hole in massive gravity

The angular velocity in this model Fig. (15) also initially exhibits a decreasing trend along the time-like unstable circular orbits and approaching the minimum β at $r = 8.8997$ and continuing towards the stable photon sphere the angular velocity starts to increase, leading to a globally non-uniform profile.

IV. CONCLUSIONS

The discovery of a non-monotonic angular velocity profile near rotating Kerr black holes—an observation fundamentally at odds with Newtonian expectations—led to the identification of a phenomenon now known as the Aschenbach effect. This behavior, rooted in two quintessential relativistic features— frame dragging and intense spacetime curvature —has become a striking indicator of general relativity’s dominance over classical physics in strongly curved geometries. This raises a pivotal question:

Is non-monotonicity in angular velocity an exclusive feature of rotating spacetimes, or can it serve as a more universal marker of relativistic behavior, even in static geometries?

This motivated investigations into non-rotating black hole models to explore whether such behavior could emerge independent of frame dragging [14, 18, 19].

In our previous study [14], we examined the mechanism responsible for this phenomenon across various ultra-compact gravitational configurations, both in the form of black holes and naked singularities. We found a consistent feature shared by all examined models [14, 18, 19]: the presence of a stable gravitational potential minimum—either local or global—which corresponds to a stable photon sphere. In naked singularity models, the absence of an event horizon naturally permits such minima. However, in black hole configurations, the existence of a stable minimum depends on its placement outside the event horizon, adding a geometric constraint.

This detection strengthens the argument that in the absence of rotational frame-dragging, the emergence of non-monotonicity in angular velocity can still arise due to spacetime curvature alone, provided the geometry allows for appropriate potential extrema. However, this condition is rare among conventional black hole solutions.

Following the analysis of the 4D Einstein–Gauss–Bonnet Massive Gravity model, alongside results reported in [19], we posed a new question:

Can the architectural framework of black holes in Massive Gravity theories accommodate the necessary conditions for Aschenbach-like phenomena?

To address this, we investigated three distinct black hole models within the context of Massive Gravity. Our findings showed that, for some range of parametric configurations (though not for all parameters), Aschenbach-like behavior was reproducible in each case. This provides compelling support for the idea that electromagnetic interaction coupled with Massive Gravity dynamics can yield black hole architectures that naturally support non-monotonic angular velocity profiles. Since the concept of a photon sphere is intrinsically tied to the framework of general relativity and lacks any classical analogue, both the original Aschenbach effect in rotating spacetimes and the Aschenbach-like phenomenon in static configurations may be considered observable signatures of general relativistic dynamics.

Finally, it is crucial to emphasize, however, that despite sharing the trait of angular velocity variability:

- In rotating black holes, the phenomenon arises from the interplay of frame dragging and strong gravity.
- In static black holes, it is governed by the presence of a minimum in the effective potential outside the horizon.

This fundamental difference in origin justifies the terminological distinction: we refer to the static case as exhibiting an "Aschenbach-Like" effect.

-
- [1] Kerr RP. Gravitational field of a spinning mass as an example of algebraically special metrics. *Physical review letters*. 1963 Sep 1;11(5):237.
- [2] Lense J, Thirring H. Über den Einfluß der Eigenrotation der Zentralkörper auf die Bewegung der Planeten und Monde nach der Einsteinschen Gravitationstheorie. *Physikalische zeitschrift*. 1918;19:156.
- [3] Mashhoon B, Hehl FW, Theiss DS. On the Influence of the Proper Rotation of Central Bodies on the Motions of Planets and Moons According to Einstein's Theory of Gravitation. *General Relativity and Gravitation*. 1984 Aug;16(8):727-41.
- [4] Carter B. Global structure of the Kerr family of gravitational fields. *Physical Review*. 1968 Oct 25;174(5):1559.
- [5] Abramowicz MA, Fragile PC. Foundations of black hole accretion disk theory. *Living Reviews in Relativity*. 2013 Dec;16(1):1.
- [6] Thorne KS. Disk-accretion onto a black hole. II. Evolution of the hole. *Astrophysical Journal*, Vol. 191, pp. 507-520 (1974). 1974
- [7] Aschenbach B. Measuring mass and angular momentum of black holes with high-frequency quasi-periodic oscillations. *Astronomy , Astrophysics*. 2004 Oct 1;425(3):1075-82.
- [8] De Villiers JP, Hawley JF. Global general relativistic magnetohydrodynamic simulations of accretion tori. *The Astrophysical Journal*. 2003 Aug 1;592(2):1060.
Van der Klis M. Fourier techniques in X-ray timing. In *Timing neutron stars 1989* (pp. 27-69). Dordrecht: Springer Netherlands.
Balbus SA, Hawley JF. A powerful local shear instability in weakly magnetized disks. I-Linear analysis. II-Nonlinear evolution. *Astrophysical Journal*, Part 1 (ISSN 0004-637X), vol. 376, July 20, 1991, p. 214-233. 1991 Jul;376:214-33.
-Ingram A, Done C. A physical model for the continuum variability and quasi-periodic oscillation in accreting black holes. *Monthly Notices of the Royal Astronomical Society*. 2011 Aug 11;415(3):2323-35.
- [9] Novikov ID, Thorne KS. *Astrophysics of black holes. Black holes (Les astres occlus)*. 1973 Jan;1:343-450.
Shakura NI, Sunyaev RA. Black holes in binary systems. Observational appearance. *Astronomy and Astrophysics*, Vol. 24, p. 337-355. 1973;24:337-55.
Shakura NI, Sunyaev RA. Black Holes in Binary Systems: Observational Appearances. In *Symposium-International Astronomical Union 1973 Jan* (Vol. 55, pp. 155-164). Cambridge University Press.
Abramowicz MA, Fragile PC. Foundations of black hole accretion disk theory. *Living Reviews in Relativity*. 2013 Dec;16(1):1.
- [10] Zanotti O, Rezzolla L, Font JA. Quasi-periodic accretion and gravitational waves from oscillating 'toroidal neutron stars' around a Schwarzschild black hole. *Monthly Notices of the Royal Astronomical Society*. 2003 May 21;341(3):832-48.
De Villiers JP, Hawley JF. Global general relativistic magnetohydrodynamic simulations of accretion tori. *The Astrophysical Journal*. 2003 Aug 1;592(2):1060.
Fragile PC, Blaes OM, Anninos P, Salmonson JD. Global general relativistic magnetohydrodynamic simulation of a tilted black hole accretion disk. *The Astrophysical Journal*. 2007 Oct 10;668(1):417.
Stuchlík Z, Slaný P. Equatorial circular orbits in the Kerr–de Sitter spacetimes. *Physical Review D*. 2004 Mar 1;69(6):064001.
- [11] Kinch BE, Schnittman JD, Noble SC, Kallman TR, Krolik JH. Spin and accretion rate dependence of black hole X-ray spectra. *The Astrophysical Journal*. 2021 Dec 6;922(2):270.
Reynolds CS, Nowak MA. Fluorescent iron lines as a probe of astrophysical black hole systems. *Physics Reports*. 2003 Apr 1;377(6):389-466.
Bardeen JM, Press WH, Teukolsky SA. Rotating black holes: locally nonrotating frames, energy extraction, and scalar synchrotron radiation. *Astrophysical Journal*, Vol. 178, pp. 347-370 (1972). 1972 Dec;178:347-70.
- [12] Schnittman JD, Krolik JH. X-ray polarization from accreting black holes: the thermal state. *The Astrophysical Journal*. 2009 Jul 30;701(2):1175.
- [13] Misner, C. W., Thorne, K. S., Wheeler, J. A. (1973). *Gravitation*. W. H. Freeman and Company.
Chandrasekhar, Subrahmanyan, and Kip S. Thorne. "The mathematical theory of black holes." (1985): 1013-1015.
Frolov, V. P., Novikov, I. D. (1998). *Black Hole Physics: Basic Concepts and New Developments*. Springer.
- [14] Afshar MA, Sadeghi J. Mechanisms behind the Aschenbach effect in non-rotating black hole spacetime. *Annals of Physics*. 2025 Mar 1;474:169953.
- [15] Afshar MA, Sadeghi J. Effective potential and topological photon spheres: a novel approach to black hole parameter classification. *Chinese Physics C*. 2025 Mar 1;49(3):035107.
Sadeghi J, Afshar MA, Gashti SN, Alipour MR. Thermodynamic topology and photon spheres in the hyperscaling violating black holes. *Astroparticle Physics*. 2024 Apr 1;156:102920.
- [16] Sadeghi J, Afshar MA. The role of topological photon spheres in constraining the parameters of black holes. *Astroparticle Physics*. 2024 Oct 1;162:102994.
- [17] Cunha PV, Berti E, Herdeiro CA. Light-ring stability for ultracompact objects. *Physical review letters*. 2017 Dec 22;119(25):251102.

- [18] Wei SW, Liu YX. Aschenbach effect and circular orbits in static and spherically symmetric black hole backgrounds. *Physics of the Dark Universe*. 2024 Feb 1;43:101409.
- [19] Yerra PK, Mukherji S, Bhamidipati C. Static spheres and Aschenbach effect for black holes in massive gravity. *Physical Review D*. 2025 Jun 15;111(12):124018.
- [20] Cunha PV, Herdeiro CA. Stationary black holes and light rings. *Physical Review Letters*. 2020 May 8;124(18):181101.
- [21] Wei SW. Topological charge and black hole photon spheres. *Physical Review D*. 2020 Sep 15;102(6):064039.
- [22] Delgado JF, Herdeiro CA, Radu E. Equatorial timelike circular orbits around generic ultracompact objects. *Physical Review D*. 2022 Mar 15;105(6):064026.
- [23] Afshar MA, Sadeghi J. Mutual Influence of Photon Sphere and Non-Commutative Parameter in Various Non-Commutative Black Holes: Part I-Towards evidence for WGC. arXiv preprint arXiv:2411.09557. 2024 Nov 14.
- [24] Afshar MA, Sadeghi J. WGC as WCCC protector: The synergistic effects of various parameters in non-commutative black holes for identifying WGC candidate models. *Nuclear Physics B*. 2025 May 1;1014:116872.
- [25] De Rham C. Massive gravity. *Living reviews in relativity*. 2014 Dec;17(1):1-89.
- [26] Fierz M, Pauli WE. On relativistic wave equations for particles of arbitrary spin in an electromagnetic field. *Proceedings of the Royal Society of London. Series A. Mathematical and Physical Sciences*. 1939 Nov 28;173(953):211-32.
- [27] van Dam H, Veltman M. Massive and mass-less Yang-Mills and gravitational fields. *Nuclear Physics B*. 1970 Sep 15;22(2):397-411.
- [28] Vainshtein AI. To the problem of nonvanishing gravitation mass. *Physics Letters B*. 1972 May 1;39(3):393-4.
- [29] Boulware DG, Deser S. Inconsistency of finite range gravitation. *Physics Letters B*. 1972 Jun 26;40(2):227-9.
De Rham C, Gabadadze G. Generalization of the Fierz-Pauli action. *Physical Review D—Particles, Fields, Gravitation, and Cosmology*. 2010 Aug 15;82(4):044020.
De Rham C, Gabadadze G, Tolley AJ. Resummation of massive gravity. *Physical Review Letters*. 2011 Jun 10;106(23):231101.
- [30] Hassan SF, Rosen RA. Resolving the ghost problem in nonlinear massive gravity. *Physical review letters*. 2012 Jan 27;108(4):041101.
- [31] Vegh D. Holography without translational symmetry. arXiv preprint arXiv:1301.0537. 2013 Jan 3.
Volkov MS. Exact self-accelerating cosmologies in the ghost-free massive gravity: $i\epsilon$ format? $i\epsilon$ The detailed derivation. *Physical Review D—Particles, Fields, Gravitation, and Cosmology*. 2012 Nov 15;86(10):104022.
Chamseddine AH, Volkov MS. Cosmological solutions with massive gravitons. *Physics Letters B*. 2011 Oct 25;704(5):652-4.
- [32] Nam CH. Non-linear charged AdS black hole in massive gravity. *The European Physical Journal C*. 2018 Dec;78(12):1016.
- [33] Ayon-Beato E, Garcia A. The Bardeen model as a nonlinear magnetic monopole. *Physics Letters B*. 2000 Nov 9;493(1-2):149-52.
- [34] Singh BK, Singh RP, Singh DV. Extended phase space thermodynamics of Bardeen black hole in massive gravity. *The European Physical Journal Plus*. 2020 Oct;135(10):1-3.
- [35] Ali MS, Ghosh SG. Exact d-dimensional Bardeen-de Sitter black holes and thermodynamics. *Physical Review D*. 2018 Oct 15;98(8):084025.
- [36] Singh DV, Ghosh SG, Maharaj SD. Bardeen-like regular black holes in 5D Einstein–Gauss–Bonnet gravity. *Annals of Physics*. 2020 Jan 1;412:168025.
- [37] Kumar A, Singh DV, Ghosh SG. D-dimensional Bardeen–AdS black holes in Einstein–Gauss–Bonnet theory. *The European Physical Journal C*. 2019 Mar;79(3):275.
- [38] Nam CH. Non-linear charged AdS black hole in massive gravity. *The European Physical Journal C*. 2018 Dec;78(12):1016.
- [39] Panah BE. Black hole solutions in theory of ModMax-dRGT-like massive gravity. *Physics Letters B*. 2025 Jul 7:139711.